

# A consensus protocol for the in silico optimisation of antibody fragments

## Supplementary Information

Miguel A. Soler,<sup>†,‡</sup> Barbara Medagli,<sup>¶</sup> Marta S. Semrau,<sup>§</sup> Paola Storici,<sup>§</sup> Gregor  
Bajc,<sup>||</sup> Ario de Marco,<sup>⊥</sup> Alessandro Laio,<sup>\*,†,#</sup> and Sara Fortuna<sup>\*,¶</sup>

<sup>†</sup>*International School for Advanced Studies (SISSA), Via Bonomea 265, 34136, Trieste,  
Italy*

<sup>‡</sup>*Italian Institute of Technology (IIT), Via Melen 83, B Block, 16152, Genova, Italy*

<sup>¶</sup>*Department of Chemical and Pharmaceutical Sciences, University of Trieste, Via L.  
Giorgieri 1, 34127 Trieste, Italy*

<sup>§</sup>*Structural Biology Laboratory, Elettra - Sincrotrone Trieste S.C.p.A. SS 14 - km 163,5 in  
AREA Science Park, 34149 Trieste, Italy*

<sup>||</sup>*Department of Biology, Biotechnical Faculty, University of Ljubljana, Jamnikarjeva 101,  
1000 Ljubljana, Slovenia*

<sup>⊥</sup>*Laboratory of Environmental and Life Sciences, University of Nova Gorica, Vipavska  
cesta 13, SI-5000, Rožna Dolina (Nova Gorica), Slovenia*

<sup>#</sup>*The Abdus Salam International Centre for Theoretical Physics (ICTP), Strada Costiera  
11, 34151 Trieste, Italy*

E-mail: laio@sissa.it; s.fortuna@units.it

# S1. Starting structure

**VHH modelling.** We modelled the starting VHH **D9** by homology modelling. To identify a suitable template we searched the PDB database with BLAST, E-Value Cutoff 10.0, and Sequence Identity Cutoff 80%, for similar frameworks of **D9**, and with loops of the same length. Thus, we removed from the set sequences with (i) insertions in the final part of the framework, (ii) length of the first CDR different than 7 amino acids, (ii) length of the third CDR larger than 14 amino acids. Among the 7 remaining sequences we chose the first three with the lowest resolution and the lowest B-factor, namely 2X10,<sup>1</sup> 3TPK,<sup>2</sup> and 4POY.<sup>3</sup> The sequence alignments to the experimental sequence show at maximum 14 point mutations in the framework. Nevertheless, no meaningful differences in the backbone were observed after their structural alignment.<sup>4</sup> Therefore, we employed all three structures as templates for modelling the VHH D9. Mutations and insertions were performed with DeepView - Swiss-PdbViewer 4.1.<sup>5</sup> We thus relaxed each model, add water, and run 100 ns MD simulations following the same protocol detailed in the Section S8 (Methods). We chose for subsequent analysis the model with the lowest potential energy as estimated along the last 40 ns of each simulation, namely the one obtained from 4POY (Fig. S1a). Moreover, the backbone root mean square deviation (RMSD, Fig. S1b) shows that the chosen model is stable over time, as its RMSD value remains smaller than 0.1 nm along the trajectory. Likewise, the root mean square fluctuation (RMSF, Fig. S1c) is greater than 0.1 nm only in the CDR loops.

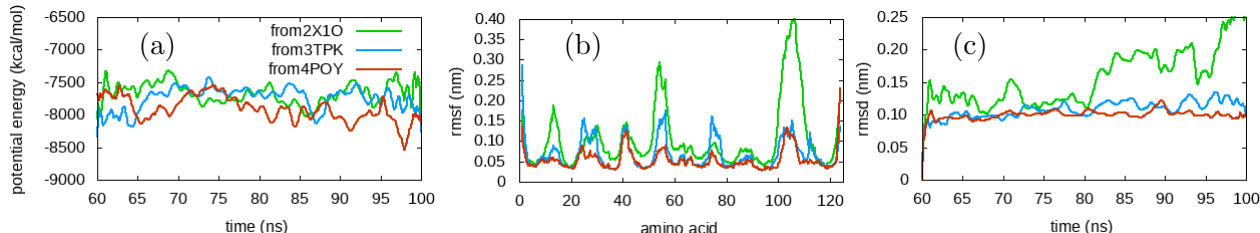


Figure S1: (a) potential energy (b) Backbone RMSD, and (c) backbone RMSF calculated over the last 40 ns of 100ns long MD simulation of **D9** built from template 2X10 (green), 3TPK (blue), and 4POY (red).

**HER2 modelling.** HER2 domain 533-629 was extracted from the PDB 3N85<sup>6</sup> (labelled 511-607 in the PDB file). The structure was energetically minimized and subsequently subjected to a 250ns MD simulation in water solution (see further details in Section S8. Methods). The RMSD analysis in Fig. S2a shows that HER2 domain achieved a stable conformation. The terminal fragment (residues 561-607) backbone alignment between the first and last snapshot has RMSD = 0.18nm Fig. S2b.

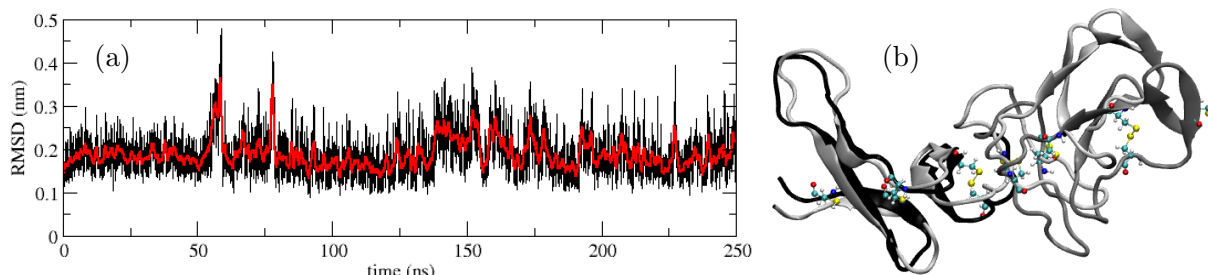


Figure S2: (a) HER2 backbone RMSD (b) First (white) and last (black/gray) Her2 conformation, the domain employed for subsequent modelling is highlighted (black) as well as the cysteins holding the system together. Residues 561-607 backbone atoms has been aligned with RMSD = 0.18nm

**D9/HER2 docking.** Since VHH **D9** has been experimentally shown to be displaced by Trastuzumab, it is known that they share the same binding site. Thus, we performed the docking between the resulting **D9** and the Trastuzumab HER2 binding site<sup>7</sup> by employing the HADDOCK<sup>8</sup> webserver “easy interface”. The protein structures employed are those obtained at the end of their respective MD simulations. We defined the “system dependent active residues” for **D9** as their CDR, while for HER2 active residues were those in contact with Trastuzumab:<sup>7</sup> 579-583, 592-595, and 615-625.

**D9/HER2 MD simulation.** The **D9**-HER2 complex obtained from docking underwent two minimizations, first without solvent, and a second one after placing the minimized complex in the cubic box with a water layer of 0.7 nm and Na+ Cl- ions to neutralize the system. Subsequently, we performed a 250 ns MD simulation at 300 K. The root mean

square deviation of the VHH-protein interface (IRMSD) with respect to the center of the most populated cluster in the last 100 ns configurations shows that the binding structure must undergo important rearrangements until achieving a stable conformation at 150-200 ns (see Fig S3). Further analysis of the binding affinity of the complex can be found in Ref.<sup>4</sup> The final snapshot at 250 ns of the complex structure was selected for the next stage.

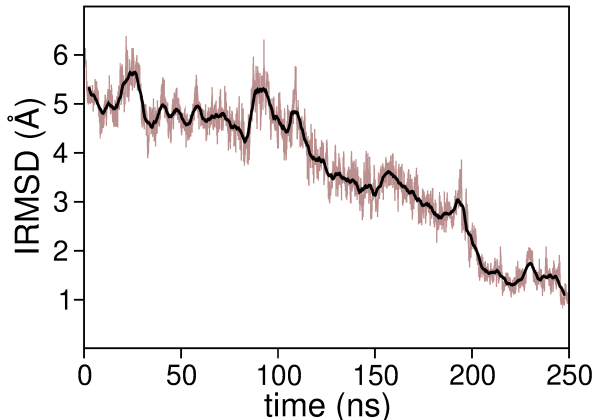


Figure S3: Evolution of the root mean square deviation of the **D9**-HER2 interface with running averages over 1 ns (black solid line).

**D9/HER2 modelling.** In order to reduce the simulation box size the HER2 domain was cleaved, by excluding the regions which were not participating in the binding, and keeping the 583-629 residues (561-607 in the PDB file), and the complex was placed in a triclinic box of 73x53x45 Å, where the binding orientation was placed along the  $x$  axis. Water molecules and 5 Na atoms were added to the simulation box to achieve the neutral charge of the system. In order to keep the orientation of the complex in the simulation box, the position of the center of mass of **D9** was fixed by restraining the position of the backbone atom N of Trp35, while the movement of the center of mass of HER2 was restricted in the  $y$  and  $z$  plane by restraining in this plane the displacement of the backbone atom N of Cys601 (see Fig. S4a). A harmonic force constant of  $5 \times 10^5 \text{ kJmol}^{-1}\text{nm}^{-2}$  was employed for each involved coordinate. Moreover, a cutoff of 8 Å was used for the electrostatic and Van der Waals non-bonded interactions. The conformation of the resulting complex was ultimately

tested by performing 100 ns MD simulation of the cleaved complex in water at 300 K. The low IRMSD values obtained with respect to the initial configuration (in the same order as those showed in Fig. S3 for **D9**-HER2 complex after achieving the stable conformation) confirmed us the stability of the binding conformation of the **D9**-HER2 complex (see Fig. S4b).

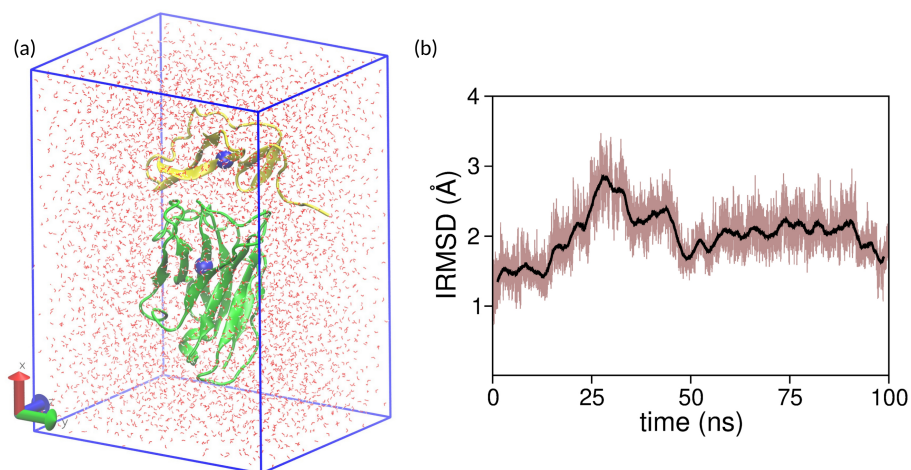


Figure S4: (a) Simulation box used for the VHH optimization. Two N atoms (highlighted in blue with their van der Waals spheres) were restrained to keep the system orientation. (b) Evolution of the root mean square deviation of the **D9**-HER2 interface with running averages over 1 ns (black solid line).

## S2. Optimization of consensus threshold

Avoiding the structure of the molecule get trapped in a local minimum is one of the main issues that every energy optimization algorithm has to deal with. In our algorithm the binding affinity is not evaluated as a single score value, as in most of typical optimization algorithms, but as a vector of binding scores. Moreover, the consensus criterion establishes that one mutation is accepted if at least  $T$  binding scores are improved by the mutation. Thus, there are  $\binom{N_s}{T}$  possible combinations to achieve this criterion. Although a higher number of scoring functions allows a higher number of combinations to achieve the consensus criterion, this will also require a higher number of scoring functions to be computed and optimized at the same time. The other alternative to optimize the maximum number of combinations, which avoid that mutations get trapped, without losing the ability of improving the binding affinity in all scoring functions is the optimization of the consensus threshold  $T$ .

As we employed 6 different scoring functions, we performed four runs of the design algorithm changing only the value of  $T = 2, 3, 4, 5$ . In order to compare the results obtained in all runs, we rank all binding scores of the accepted mutations obtained in the runs, being  $r_k^i$  the rank of a complex  $i$  according to the scoring function  $k$ . Likewise,  $r_k^i$  can be normalized as

$$\hat{r}_k^i = \frac{r_k^i}{N} \quad (1)$$

where  $N$  is the total number of accepted mutations obtained in the runs. Finally, the global rank of a complex  $i$  is defined as

$$R^i = \sum_{k=1, N_s} \frac{\hat{r}_k^i}{N_s} \quad ; \quad i = 1, N \quad (2)$$

Therefore, if the ranks of a certain configuration  $i$  are consistently low for all the scoring functions then  $R^i$  is small. In Figure S5 we show the ranking score of the VHH/HER2 complexes obtained from four different design simulations in which consensus threshold is set

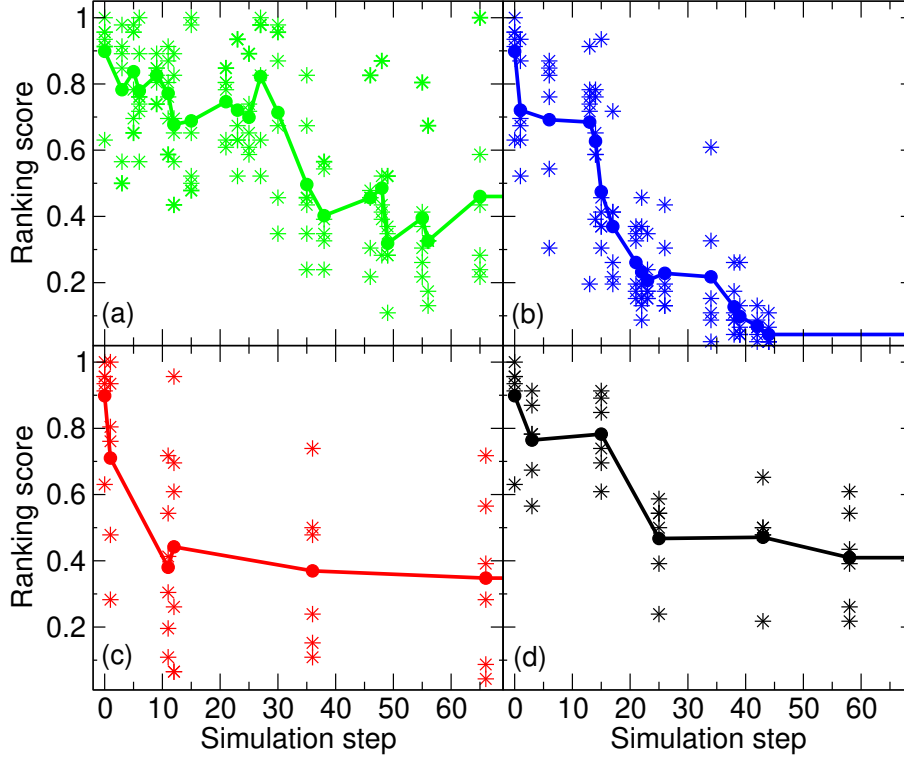


Figure S5: Global (circle and line) and individual (star) ranking scores of the bindings between VHH mutants and HER2 obtained along the simulations, from (a) to (d), with  $T = 2, 3, 4, 5$ , respectively.

to  $T = 2, 3, 4, 5$ , respectively. The lowest  $R_i$  values are found in the VHH/HER2 complexes optimized with  $T = 3$ . More important, all the individual binding scores in those mutants have been optimized, since  $\hat{r}_k^i$  values are also low for these complexes. Only when  $T = 3$  the variance of the ranks is small at the end of the optimization run, implying that the algorithm finds sequences for which  $\hat{r}_k^i$  is consistently small for all scoring functions. When a lower  $T$  is used, i.e.  $T = 2$ , the acceptance of new mutations is slightly higher, but the individual ranks of all scoring functions do not achieve low values for the same accepted mutations. Likewise, in simulations with higher  $T$ , i.e.  $T = 4, 5$ , the number of accepted mutants is clearly lower due to the strict criterion. Therefore, it would be necessary to perform longer simulations to achieve the optimization in all scoring functions.

To gain a better understanding of the differences obtained by employing  $T = 2, 3$ , we calculated the Spearman correlation coefficients between the binding score ranks of the

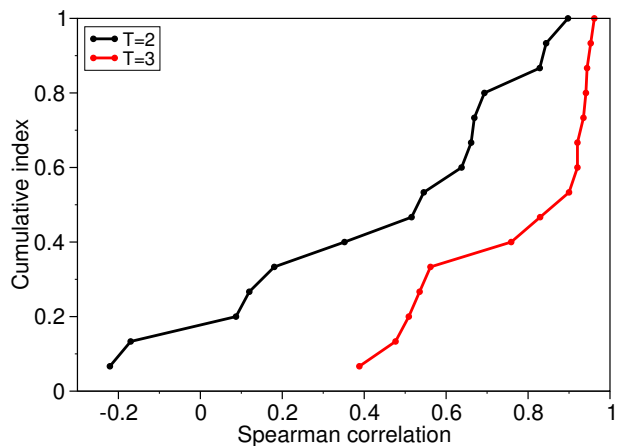


Figure S6: Spearman correlation between binding scores of the VHH/HER2 complexes obtained along the simulations with  $T = 2, 3$ , sorted by ascending order.

VHH/HER2 complexes obtained in each design simulation for two different scoring functions. Taking into account that we used 6 scoring functions, for each simulation we obtained the half-side correlation matrix of 15 elements. In the Figure S6 we compare the correlation values obtained from simulations with  $T = 2, 3$ , sorted by ascending order. According to these results, all correlations between scoring functions obtained from  $T = 3$  simulations are clearly higher than those obtained by using  $T = 2$ . The biggest differences are found in the lowest correlation values, where for  $T = 2$  there are correlations between scoring functions with negative values, corresponding to Pie\*Pisa/Bluues and Pie\*Pisa/Haddock, while the lowest correlation obtained with  $T = 3$  is around 0.4. Therefore, these results confirm that the optimal consensus threshold in our system is  $T = 3$ , since only by using  $T = 3$  the optimization is reached for all scoring functions.

### S3. Design of peptides as binders of HER2

We show that our computational design protocol can be extended to other binders by carrying out the optimisation of 15-aa cyclic peptides for the recognition of aa533-629 HER2 fragment.

**Initial peptide structure.** We took advantage of the optimisation of the VHH **D9** to model the sequence and binding conformation of the starting peptide. Thus, we followed the following computational steps depicted in Fig. S7: (i) the main interacting residues, i.e. 13 amino acids in this case, of VHH **44** were identified and isolated; (ii) they were grafted onto a 15-aa cyclic peptide, placing the Cys-Cys extremes of the chain in the longest gap between two VHH residues, and the complex underwent a 20ns MD simulation to stabilize the complex; (iii) finally, we performed the docking between the resulting peptide conformation and the fragment 533-629 of HER2. For this step, we selected the HER2 conformation from the MD simulation described in Section S1 (HER2 modelling) that had the lowest RMSD value with respect to the cleavaged HER2 fragment used initially. The resulting complex underwent one last time a 100 ns MD simulation, and the last complex pose of the trajectory

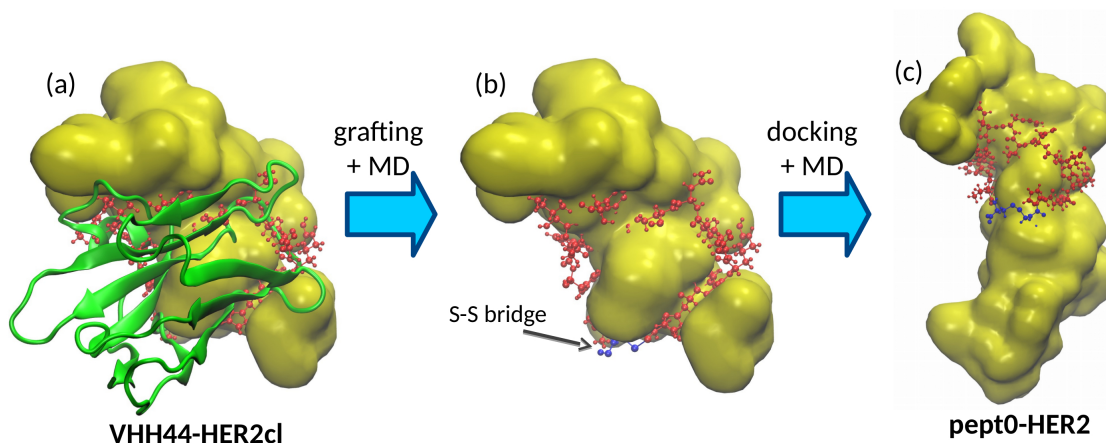


Figure S7: (a) The **44-HER2** complex was employed to identify the principal 13 interacting VHH residues (in red). (b) They were grafted onto a 15-aa cyclic peptide, whose both ends were Cys that close the ring with a S-S bridge (in blue). (c) The resulting peptide conformation was docked onto the same binding site of 533-629 HER2 fragment and the resulting complex underwent a MD simulation.

was used as starting complex structure for the design simulation.

**Peptide design results.** We used then our *in silico* mutagenetic protocol (freely available at <https://github.com/migsoler/BINDesignER>) to optimise the binding affinity of the peptide-HER2 complex by evaluating iteratively the impact of single random mutations in the 13 residues of the peptide, i.e. extreme Cys residues are excluded to guarantee the cycle structure. We followed the same computational protocol described for the optimisation of VHH **D9**. A 100-step optimisation of the peptide-HER2 complex is shown in Fig. S8a. By using the same threshold in the consensus algorithm,  $T = 3$ , the iterative accepted mutations lead to the gradual increase of the binding affinity for all 6 scoring functions. Despite the clear differences between peptides and VHHS as binders, in both systems a consensus is achieved among all scoring functions allowing to identify optimum binders. Subsequently

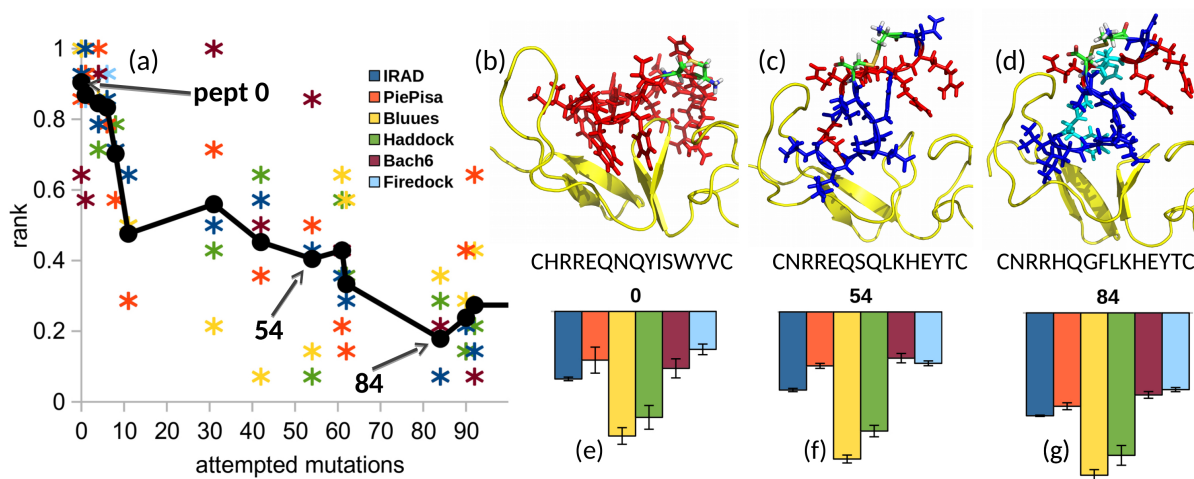


Figure S8: (a) Global (black circles and line) and scoring-function specific (star) ranking scores of the bindings between peptide mutants and HER2 as obtained along the optimization with  $N_s = 6$ ,  $T = 3$ . Two selected mutants are indicated by arrows; (b-d) simulation snapshots of the three selected complexes and their respective peptide sequences. Peptide amino acids are highlighted as follows: the same as in **pept 0** (red), mutated at step 54 with respect to **pept 0** (blue), mutated at step 84 with respect to **54** (cyan); (e-g) binding scores averaged over MD simulations of the selected peptide/HER2 complexes, interval 100-200ns, error bars are standard deviations calculated by block analysis. In this representation the units of the different scoring functions have been rescaled in order to make the relative variations visible.

we selected two peptide-HER2 complexes: the first ranking complex **84**, and the complex **54** randomly chosen along the optimisation path, in the middle of the ranking list. On these we performed 200 ns MD simulations in water solvent at 330 K. A comparison of their binding conformations with the one of **pept 0** reveals a meaningful conformational change of the peptide structures, in which the mutated residues are interacting with HER2 while the charged residues RRE, preserved from **pept 0**, are solvent exposed (Figure S8b-d). Their binding score averages<sup>4</sup> calculated over the last 100 ns further confirm to bind stronger than the original **pept 0** by almost all SFs for **54** and clearly all SFs for **84** (Figure S8e-g). Overall, we showed that our *in silico* consensus-based protocol is able to optimize different binder systems, obtaining a good performance for all SFs when a consensus threshold is set to half of the total number of SFs.

## S4. Comparison to Metropolis algorithm

In order to compare the improvement achieved with the implementation of the consensus acceptance criterion, we performed an equivalent design simulation, but employing in this case our previous mutation acceptance algorithm<sup>9</sup> based on a Metropolis criterion:

$$P_{\text{acc}} = \min[1, \exp[-(E_{\text{new}} - E_{\text{old}})/T_{\text{MC}}]] \quad (3)$$

where  $E_{\text{old}}$  is the binding score of the old configuration,  $E_{\text{new}}$  is that of the attempted mutation, and  $T_{\text{MC}}$  is a parameter for tuning the Metropolis acceptance probability  $P_{\text{acc}}$ . We chose the binding scores computed by the Haddock scoring function, as it showed high accuracy for these systems in our recent work,<sup>4</sup> and  $T_{\text{MC}} = 4$ , which restricts the mutation acceptances practically to those that improves the binding affinity. In Figure S9 we compare the binding scores computed by all 6 scoring functions of the VHH/HER2 complexes obtained along the design simulations employing the  $T = 3$  consensus criterion and the Metropolis criterion algorithms. The complexes obtained along the simulation with Metropolis criterion show the

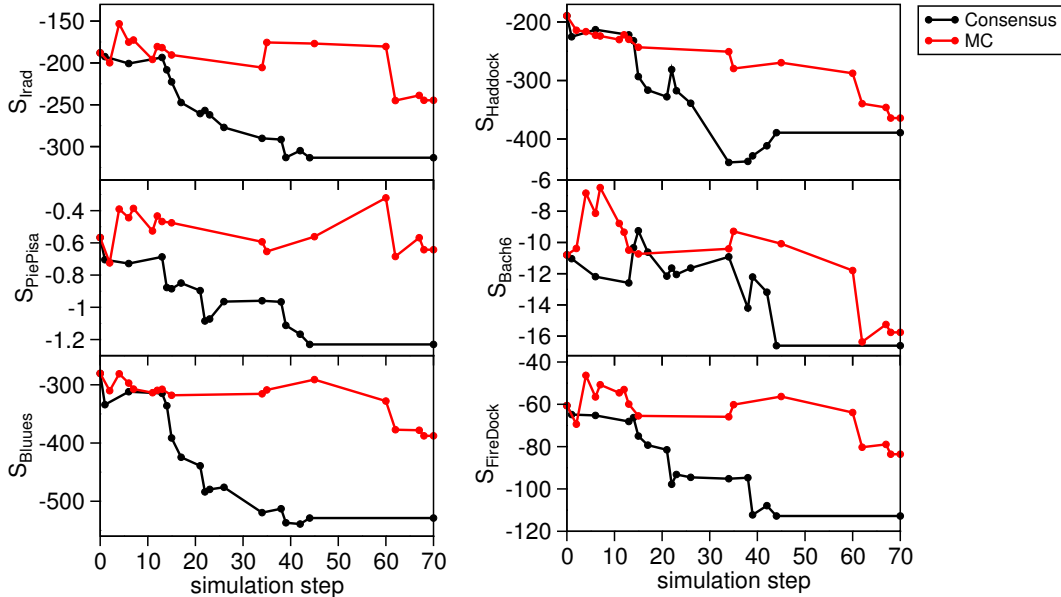


Figure S9: Binding scores of the VHH/HER2 complexes obtained along the simulations with the  $T = 3$  consensus criterion algorithm and with the Metropolis criterion algorithm.

gradual optimization of the Haddock binding score until achieving similar values as those obtained in the consensus design at the end of the simulation. However, for other scoring functions the trend along the simulation is just random. Only by chance, the mutation performed at step 62 is the only one favorable for all scoring functions. Thus, the binding score values achieved with the Metropolis criterion is certainly higher than those obtained by using the consensus criterion for the rest of the scoring functions (with the exception of Bach6, which have similar values too). Overall, these results show the efficiency to optimize globally a set of scoring functions by employing the consensus acceptance criterion.

## S5. Sequences

The starting **D9** sequence reads as follow:

MAEVQLQASGGGFVQPGGSLRLSCAA SGGTSTTDG MGWFRQAPGKEREFVSAIS SDASQEE

YYADSVKGRFTISRDNKNTVYLMNSLRAEDTATYYCA QYAFLDQEEPVIISW YWGQGTQVTVSS

Table S1: Selected VHH CDR1 sequences, and their binding affinity rankings output of the design algorithm ( $R_i$ ) and ranking averaged along the molecular dynamics screening ( $R_i^{MD}$ ).

VHH	CDR1 sequence	$R_i$ (order)	$R_i^{MD}$ (order)
<b>D9</b>	<b>SGGTSTTD</b>	<b>0.90</b>	<b>0.95</b>
<b>44</b>	HRREQNQD	0.04(1)	0.09(1)
42	QRREQNQD	0.07(2)	0.22(2)
39	QRREQNAD	0.10(3)	0.42(5)
38	QRREQNGD	0.13(4)	0.38(4)
23	QRREQDTD	0.21(5)	0.69(9)
34	QRREQNTD	0.22(6)	0.58(6)
26	QRREQNTD	0.23(7)	0.63(8)
22	QRTEQDTD	0.23(8)	0.58(7)
<b>21</b>	QRGEQDTD	0.26(9)	0.33(3)

## S6. Binding affinity screening

In order to confirm the enhanced binding affinity of the VHH mutants obtained by our design algorithm towards the target protein we selected the best solutions obtained by the design simulation and performed 200 ns MD simulations of VHH/HER2 complexes in water solution at 330 K. The binding scores given by the 6 scoring functions were analyzed along the trajectories.

As initial structures to be used in long-time MD runs, we employed the final structure of the selected complexes obtained in the design algorithm. In Figure S10 we show the evolution of the 6 binding scores of some representative complexes, **44**, **34**, and **D9**/HER2 complexes, along the trajectories.

The binding scores of most VHH/HER2 complexes are stable along the simulation and clearly present lower values than those obtained for the **D9**/HER2 complex. Even for those mutants located in low rank positions, such as VHH **34**, their binding score curves evolve at lower values than those obtained for VHH **D9**. In order to compare numerically the binding affinities of the designed complexes, we followed the same computational protocol

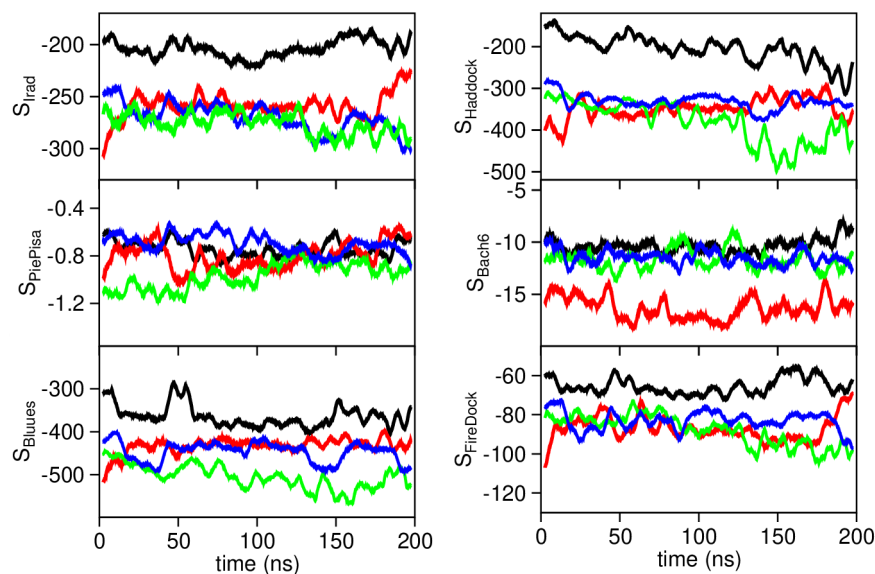


Figure S10: Evolution of binding scores of selected VHH/HER2 complexes: **D9**(black), **44**(red), **42** (blue), and **21** (green).

developed in Ref.<sup>4</sup> by computing the binding score averages over the last 100 ns of the MD trajectories for each scoring function curve. In Figure S11, we show the binding score averages of **D9**/HER2 and the selected VHH/HER2 complexes grouped by each scoring function. First, the small standard deviations observed for most of binding scores confirm the high stability of the binding estimated for all designed complexes. More important, the binding score averages obtained in the MD trajectories follow in general the same growing order established by the global score rank computed during the design runs. Indeed, almost all score averages of VHH are lower than the one obtained for **D9**/HER2 complex for each scoring function. The exceptions are the mutants **34** and **22** in Bach6. In order to compare the global binding affinities of the analyzed complexes, we computed again the global order rank as in Eq.2, but ranking in this case the binding score averages obtained from MD trajectories,  $R_i^{MD}$  (see Table S1). These values confirm the VHH mutant **44** as the best binder obtained by our design algorithm. The Spearman correlation between the rank order obtained in the simulation runs and the one obtained by using the MD trajectories of 0.69 is certainly high. Therefore, we can consider that the approach used in our design algorithm to estimate the binding affinity of mutants towards the protein target is a good approximation.

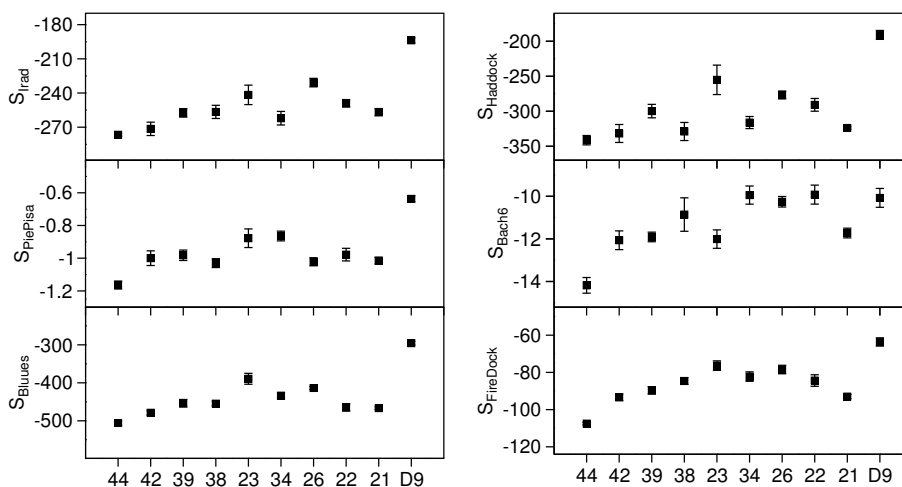


Figure S11: Binding score averages of selected VHH and **D9** complexes with HER2. Standard deviations are calculated by block analysis.

## S7. Enzyme-linked immunosorbent assay (ELISA)

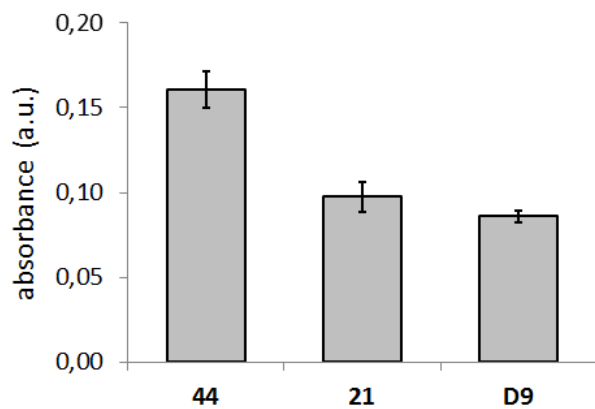


Figure S12: ELISA TEST. Absorbance at 450nm was read for the three investigated VHH: **44**, **21**, **D9**, adsorbed on a HER2 coated surface.

## S8. Methods

### S8.1 Computational.

**Molecular dynamics.** All MD simulations in this work were performed in Gromacs 5.1.2<sup>10</sup> and employed the following general parameters. Previous to every production phase, a standard 100 ps NVT + 100 ps NPT equilibration protocol was performed. A time step of 2 fs was used with the leap-frog integrator. The AMBER99SB-ILDN<sup>11</sup> force field and the water model TIP3P. Particle Mesh Ewald summation was used for long-range electrostatics. The Lincs algorithm<sup>12</sup> was employed to constraint all covalent bonds of the system. The velocity rescaling thermostat<sup>13</sup> was used to keep constant the temperature in NVT and NPT simulations while the pressure was controlled with an isotropic ParrinelloRahman barostat at 1 bar in the NPT simulations. Other specific parameters will be described in each section.

**Design algorithm.** Mutations. At each optimization step a random residue of the CDR1 (24-31) was selected and substituted by a random amino-acid (excluding Cys). The side chain of the mutated residue was reconstructed with Scwrl4.<sup>14</sup> HER2 structure was also included in the reconstruction of the mutated residue side chain as static frame atoms. Minimization and restoration of water solvent. The mutated VHH was fully relaxed by: (i) partial minimization only for the side chain of the mutated residue, while the rest of atoms of the complex *in vacuo* were kept frozen; (ii) partial minimization for the mutated amino acid and nearest neighboring residues of VHH, while the rest of the complex *in vacuo* was frozen, (iii) all water molecules returned in the box, except those closer than 2 Å of the mutated residue, and (iv) global minimization. The protocol, implemented in a bash script, is freely available at <https://github.com/migsoler/BINDesignER> Molecular dynamics. After the minimization protocol, a 100 ps NVT MD equilibration of the system is performed at 330 K. Subsequently, a 30 ns NPT MD simulation of the system is run at 330 K, the mass of water molecules was modified to 2.0 for all atoms in order to accelerate the thermodynamics.

Scoring Functions. Configurations of each mutant VHH/HER2 complex was sampled from MD simulation every 100 ps while the first 10 ns of the trajectory was discarded, obtaining a set of 100 poses. The binding affinity of each pose was then scored and the average of each scoring function was computed over the binding scores of all poses. Each scoring function parameters were configured according to the Ref.<sup>4</sup> The scores of Pie and Pisa were multiplied as recommended in Ref.<sup>15</sup> The scoring functions of FireDock<sup>16</sup> and HADDOCK v2.1<sup>17</sup> were extracted from their respective docking programs. The radii scaling parameter in FireDock was set to 0.8 as in ref.<sup>16</sup> The protonation of all histidine residues were previously defined in the HADDOCK input file according to the criterion of Gromacs. The binding score in Blues<sup>18</sup> was computed as the difference of scores between the complex and the isolated proteins. We used the option "strict\_interface" for obtaining the binding score in Bach6.<sup>19</sup>

**Molecular dynamics screening.** Selected complexes from the design as well as their respective optimized VHHs alone were placed in a cubic box with a 0.9 nm water layer and Na<sup>+</sup> Cl<sup>-</sup> ions to neutralize the system. We performed NVT and NPT equilibrations for 100 ps, followed by 250 ns NPT production run at 300 K. A cutoff of 9 Å was used for the electrostatic and Van der Waals non-bonded interactions. Configurations were sampled every 10ps. All the simulations and their analysis were run as implemented in the Gromacs package.<sup>20</sup> The poses obtained from the last 100 ns of the MD trajectories of the VHH/HER2 complexes were employed to evaluate the binding affinity following the methodology described above.

**Yield prediction.** Poses obtained from the last 100ns of the MD trajectories of the VHH monomers were used to predict the yield of each selected binder by following the methodology of Ref.,<sup>21</sup> namely: (i) clustering of VHH poses; (ii) prediction of each cluster putative aggregation hotspots; (iii) semi-flexible docking of homo-dimers testing all possible interaction combinations between the different hotspots in the monomer. The hotspots selection was performed by using the BEPPE prediction server<sup>22</sup> with softness level 4, while for the docking we employed the web interface of Haddock<sup>8</sup> with its standard parameters.

Further details can be found in Ref.<sup>21</sup>

## S8.2 Experimental procedure

**Recombinant proteins production.** The computationally generated primary sequence was converted in nucleic acid using the The Sequence Manipulation Suite,<sup>23</sup> with default parameters generating a DNA sequence with *E. coli* codon usage. The synthetic VHHs DNA sequences were purchased from the Twist Bioscience Corporation and further *E. coli* optimized using the company algorithm (San Francisco, CA, USA). The DNA fragments were cloned into pET14 Cys tag vector between NcoI and NotI recognition sites. The pET14 Cys-VHH-D9 and pET14 Cys-VHH-44 constructs were expressed in BL21 (DE3) SOX and purified as previously described.<sup>24</sup> Briefly the cell pellets of 500 ml of liquid culture, were resuspended in 25 ml of lysis buffer (20 mM Tris pH 7.9, 500 mM NaCl, 2 mM Imidazole, 5% Glycerol, 1 mg/ml lysozyme, 1 mM PMSF, 0,02 mg/ml DNase I, 10 mM MgCl<sub>2</sub>), and were homogenized after 60 min of incubation at 4°C under agitation (Invensys APV-1000, 3 cycles at 10000-12000 psi) and subsequently centrifuged (4400 x g. for time 45 min). Cleared lysates were loaded onto Ni-NTA Agarose Resin (Invitrogen), after several washes with increasing amount of imidazole (40 Resin Volumes), the proteins were eluted with 7-8 RV of 20 mM Tris pH 7.9, 500 mM NaCl, 400 mM Imidazole, 5% Glycerol, 2 mM DTT. The samples were further purified by size exclusion chromatography (SEC) on Superdex 75 10/300 (GE Healthcare) in PBS supplemented with 5% Glycerol. The fraction containing the VHHs were pooled and concentrated. DNA encoding for the ectodomain residues 23-652 of the human HER2 fused with C-terminal rabbit IgG Fc tag was cloned into pACEMam1 vector (kindly provided by I. Berger, University of Bristol, UK). The recombinant protein was expressed by transient transfection with PEI-MAX 40K (Polysciences, Inc.) in HEK293ES cells in suspension (Expression Systems), incubated for 5 days at 37°C. Exhausted medium containing the secreted proteins was clarified by centrifugation followed by filtration on 0,45µm vacuum filter system (Euroclone) and loaded on 1ml HiTrap MabSe-

lect SuRe (GE Healthcare) equilibrated with 1x PBS pH 7.4 buffer. The protein was eluted with 0.1M glycine pH 3 and immediately neutralized by adding 100 $\mu$ l of 1.5M Tris pH 8.8 per 1ml of protein fraction. Buffer exchange into 1x PBS, 1mM DTT and protein concentration was performed using Amicon Ultra centrifugal filters 30k MWCO (MerckMillipore).

**Enzyme-linked immunosorbent assay (ELISA)** 80 ng (or 0.8 pmol) of Her2 in sodium carbonate/bicarbonate pH 9.2 were immobilized in each well of a multiwell plate (Greiner) at °C ON; the day after 3 washes of 5 min in PSB-T (PBS + 0,05% Tween 20) were performed to remove any unbound protein. The sample is treated with a blocking solution (PBST 5% Milk) for 60 min; followed by the addition of 160 ng (or 10 nmol) of the various VHH in PBST 1% Milk (per well); 3 washes for 5 min in PSB-T to wash the well from the exceeding VHH. An anti 6His Antibody (Sigma Aldrich) and an anti Mouse peroxidase conjugated Antibody (Merk) were used for recognize and develop the assay according to the manufacturer suggestions. For the peroxidase reaction 3,3',5,5'-Tetramethylbenzidine (TMB, Sigma Aldrich) was used as substrate, incubated for 30 min and stopped using H<sub>2</sub>SO<sub>4</sub> The absorbance at 450 nm measured using a Tecan Infinite F200.

**Surface plasmon resonance (SPR)** The SPR experiments were performed at 25°C using a Biacore T100 (GE Healthcare); the data were fitted with a 1:1 Langmuir interaction model. HER2 ECD-Fc (96 kDa) was diluted to 50  $\mu$ g/mL in sodium acetate buffer pH 5.0 and immobilized by amine-coupling on a CM5 chip (GE Healthcare) at 1190RU on Fc4. Both the VHHs were diluted in HBS-EP+ buffer and used as analyte, with concentration ranging from 300 to 0,5  $\mu$ M, at 30  $\mu$ l/min. Concentration ranging was for D9.44 from 2000nM to 31,25nM and for D9wt from 4000 to 125 nM. The association was followed for 120 sec, and the dissociation for 80 sec. The regeneration performed using 5mM NaOH for 6s followed by buffer cycles (blank) between each concentration. The SPR measurements were performed at the Infrastructural Centre for Analysis of Molecular Interactions at the Department of Biology, University of Ljubljana (Slovenia).

## References

- (1) Van den Abbeele, A.; De Clercq, S.; De Ganck, A.; De Corte, V.; Van Loo, B.; Soror, S. H.; Srinivasan, V.; Steyaert, J.; Vandekerckhove, J.; Gettemans, J. Cell Mol Life Sci **2010**, 67, 1519.
- (2) Morgado, I. et al. Proceedings of the National Academy of Sciences **2012**, 109, 12503.
- (3) Horn, J. R.; Fanning, S. W.; Walter, R. Protein Engineering, Design and Selection **2014**, 27, 391.
- (4) Soler, M. A.; Fortuna, S.; de Marco, A.; Laio, A. Phys. Chem. Chem. Phys. **2018**, 20, 3438.
- (5) Guex, N.; Peitsch, M. C. ELECTROPHORESIS **1997**, 18, 2714.
- (6) Fisher, R. D.; Ultsch, M.; Lingel, A.; Schaefer, G.; Shao, L.; Birtalan, S.; Sidhu, S. S.; Eigenbrot, C. Journal of Molecular Biology **2010**, 402, 217.
- (7) Cho Hyun-Soo.; Mason Karen.; Ramyar Kasra X.; Stanley Ann Marie.; Gabelli Sandra B.; Denney Dan W.; Leahy Daniel J., Nature **2003**, 421, 756.
- (8) van Zundert, G.; Rodrigues, J.; Trellet, M.; Schmitz, C.; Kastritis, P.; Karaca, E.; Melquiond, A.; van Dijk, M.; de Vries, S.; Bonvin, A. Journal of Molecular Biology **2016**, 428, 720.
- (9) Soler, M. A.; Rodriguez, A.; Russo, A.; Adedeji, A. F.; Dongmo Founthum, C. J.; Cantarutti, C.; Ambrosetti, E.; Casalis, L.; Corazza, A.; Scoles, G.; Marasco, D.; Laio, A.; Fortuna, S. Phys. Chem. Chem. Phys. **2017**, 19, 2740.
- (10) Abraham, M. J.; Murtola, T.; Schulz, R.; Pll, S.; Smith, J. C.; Hess, B.; Lindahl, E. SoftwareX **2015**, 1-2, 19.

- (11) Lindorff-Larsen, K.; Piana, S.; Palmo, K.; Maragakis, P.; Klepeis, J. L.; Dror, R. O.; Shaw, D. E. Proteins: Structure, Function, and Bioinformatics **2010**, 78, 1950.
- (12) Hess, B.; Bekker, H.; Berendsen, H. J. C.; Fraaije, J. G. E. M. Journal of Computational Chemistry **1997**, 18, 1463.
- (13) Bussi, G.; Donadio, D.; Parrinello, M. The Journal of Chemical Physics **2007**, 126, 014101.
- (14) Krivov, G. G.; Shapovalov, M. V.; Dunbrack Jr., R. L. Proteins: Structure, Function, and Bioinformatics **2009**, 77, 778.
- (15) Viswanath, S.; Ravikant, D. V. S.; Elber, R. Proteins **2013**, 81, 592.
- (16) Andrusier, N.; Nussinov, R.; Wolfson, H. J. Proteins **2007**, 69, 139.
- (17) Dominguez, C.; Boelens, R.; Bonvin, A. M. J. J. J. Am. Chem. Soc. **2003**, 125, 1731.
- (18) Fogolari, F.; Corazza, A.; Yarra, V.; Jalaru, A.; Viglino, P.; Esposito, G. BMC Bioinformatics **2012**, 13, S18.
- (19) Sarti, E.; Granata, D.; Seno, F.; Trovato, A.; Laio, A. Proteins **2015**, 83, 621.
- (20) others,, et al. Bioinformatics **2013**, 29, 845.
- (21) Soler Miguel A.,; de Marco Ario,; Fortuna Sara, Sci. Rep. **2016**, 6, 34869.
- (22) Scarabelli, G.; Morra, G.; Colombo, G. Biophysical Journal **2010**, 98, 1966.
- (23) Stothard, P. Biotechniques **2000**, 28, 1102.
- (24) Djender, S.; Schneider, A.; Beugnet, A.; Crepin, R.; Desrumeaux, K. E.; Romani, C.; Moutel, S.; Perez, F.; de Marco, A. Microb. Cell. Fact. **2014**, 13, 140.